Biophysical Journal
Article

Biophysical Society

Two separate mechanisms are involved in membrane permeabilization during lipid oxidation

Min Xie,[1] Eveline H. W. Koch,[1] Cornelis A. van Walree,[1,2] Ana Sobota,[3] Andreas F. P. Sonnen,[1,4] Eefjan Breukink,[1] J. Antoinette Killian,[1] and Joseph H. Lorent[1,5,*]

[1]Membrane Biochemistry & Biophysics, Bijvoet Center for Biomolecular Research, Department of Chemistry, Utrecht University, Utrecht, the Netherlands; [2]University College Utrecht, Campusplein 1, Utrecht, the Netherlands; [3]Atmospheric Pressure Non-Thermal Plasmas and Their Interaction with Targets, Applied Physics Department, Eindhoven University of Technology, Eindhoven, the Netherlands; [4]Pathology Department, University Medical Center Utrecht, Utrecht, the Netherlands; and [5]Cellular and Molecular Pharmacology, Translational Research from Experimental and Clinical Pharmacology to Treatment Optimization, Louvain Drug Research Institute, UCLouvain, Brussels, Belgium

ABSTRACT Lipid oxidation is a universal degradative process of cell membrane lipids that is induced by oxidative stress and reactive oxygen and nitrogen species (RONS) in multiple pathophysiological situations. It has been shown that certain oxidized lipids alter membrane properties, leading to a loss of membrane function. Alteration of membrane properties is thought to depend on the initial membrane lipid composition, such as the number of acyl chain unsaturations. However, it is unclear how oxidative damage is related to biophysical properties of membranes. We therefore set out to quantify lipid oxidation through various analytical methods and determine key biophysical membrane parameters using model membranes containing lipids with different degrees of lipid unsaturation. As source for RONS, we used cold plasma, which is currently developed as treatment for infections and cancer. Our data revealed complex lipid oxidation that can lead to two main permeabilization mechanisms. The first one appears upon direct contact of membranes with RONS and depends on the formation of truncated oxidized phospholipids. These lipids seem to be partly released from the bilayer, implying that they are likely to interact with other membranes and potentially act as signaling molecules. This mechanism is independent of lipid unsaturation, does not rely on large variations in lipid packing, and is most probably mediated via short-living RONS. The second mechanism takes over after longer incubation periods and probably depends on the continued formation of lipid oxygen adducts such as lipid hydroperoxides or ketones. This mechanism depends on lipid unsaturation and involves large variations in lipid packing. This study indicates that polyunsaturated lipids, which are present in mammalian membranes rather than in bacteria, do not sensitize membranes to instant permeabilization by RONS but could promote long-term damage.

SIGNIFICANCE Oxidative stress is a common pathophysiological process that leads to the impairment of cell membranes due to the formation of oxidized lipids. Unfortunately, it is unknown how a complex mixture of oxidized lipids impairs membrane function by altering biophysical membrane properties upon lipid unsaturation. We therefore combined analytical techniques to quantify oxidized lipids and correlated their quantity to key biophysical membrane parameters. We observed two mechanisms impairing the integrity of the membrane. One is unsaturation independent and dominated by truncated lipids, produced by short-living reactive oxygen species. The second is unsaturation dependent and occurs upon formation of lipid oxygen adducts after longer incubation periods. Both mechanisms trigger the release of oxidized lipids from the membrane that could constitute signaling molecules.

INTRODUCTION

Cell membrane oxidation is a universal degradative process that can ultimately lead to the alteration of membrane properties and cell death. It is usually started by reactive oxygen and nitrogen species (RONS) that induce membrane lipid or protein oxidation in the absence of efficient oxidative defense mechanisms (1). RONS are generated during oxidative stress in pathophysiological situations or as a defense mechanism toward infectious germs in phagolysosomes of macrophages and neutrophils to kill invading microorganisms (2,3). Cold atmospheric plasma (CAP) is a relatively new technology that mimics this principle to fight bacterial infections or even cancer cells by producing large amounts of RONS in situ that can

Submitted August 29, 2023, and accepted for publication October 25, 2023.

*Correspondence: joseph.lorent@uclouvain.be

Editor: Ilya Levental.

https://doi.org/10.1016/j.bpj.2023.10.028

be directly applied to an infected wound or tumor, for instance by a plasma pen (4,5). It has been proposed that the main target of exoplasmically produced RONS is the cell membrane, whose lipids and proteins are subsequently oxidized, leading to alterations of numerous biophysical properties of the membrane that compromise its biological function (6).

In prior studies, it has been shown that lipid oxidation and its consequences for biophysical properties of membranes such as permeability or fluidity depend strongly on the lipid composition (1,7), which is largely organelle and species dependent (8,9). Although lipids in membranes of gram-positive bacteria mainly contain saturated or monounsaturated acyl chains (9), human cell membranes present a much larger distribution of unsaturations, including polyunsaturated lipids (8). Most phospholipids are asymmetrically unsaturated, containing a saturated and an unsaturated tail at the *sn-1* and *sn-2* position, respectively, whereas just a minority of phospholipids possess two saturated or two unsaturated tails (10). Polyunsaturated lipids are more sensitive to oxidative modifications (11). This is due to the formation of a pentadienyl radical, which is stabilized by the mesomeric effect. Addition of an oxygen molecule to the lipid radical can then produce a hydroperoxyl radical, which itself can react with another polyunsaturated lipid, giving rise to another lipid radical and a hydroperoxide. This radical chain reaction is called lipid peroxidation in the literature (1).

Several studies showed that the formation of lipid oxides can modulate biophysical properties of membranes and induce pore formation (7,12,13). Ytzhak et al. found that membranes containing polyunsaturated lipids were more prone to permeabilization. However, they used high concentrations of polyunsaturated lipids such as di-18:2, di-18:3, or di-18:6, which are only found at very small concentrations in cells (7,10). In a similar experiment on giant unilamellar vesicles, Bour et al. reached no definitive conclusion regarding the presence of lipid unsaturations and sensitivity to permeabilization (14). Usually, the effects on membrane properties and integrity depend on the individual oxidized lipid species that are created. There are strong indications that secondary cleavage products such as lipid aldehydes and carboxylic acids have a stronger effect on permeabilization, whereas lipid hydroperoxides drastically change the area/lipid ratio and induce lipid phase separation but seem to be less effective in permeabilizing membranes (12,13,15–17).

Although the effects of single oxidized lipid species on certain biophysical properties have become apparent, it is not clear how a complex combination of oxidized lipids, which is biologically more relevant, would induce changes to membrane properties. This is mainly due to the difficulty of simultaneously quantifying each oxidized lipid species. A comparison on how symmetric (e.g., PC(18:1/18:1)) versus asymmetric (e.g., PC(16:0/18:1)) monounsaturated or polyunsaturated lipids (Fig. 1 *B*) sensitize membranes to oxidative damage is also lacking. Further, the distinction between direct damage to membranes by RONS versus long-term effects from continuous reactions such as lipid peroxidation after post-incubation periods is often omitted. This is biologically highly relevant since an initial small-scale damage could eventually develop into serious membrane alterations in the absence of efficient antioxidant repair mechanisms. In this perspective, we investigate short- and long-term permeabilization and membrane packing in parallel to molecular changes induced by RONS that are produced in situ by CAP in large unilamellar vesicles (LUVs) composed of symmetric and asymmetric mono- and polyunsaturated lipids. To determine the enounced properties, we use a combination of biophysical, biochemical, and analytical approaches described hereunder.

MATERIALS AND METHODS

Chemicals and reagents

Argon (purity 5.0) was ordered from Linde (Ireland). 1-Palmitoyl-2-oleoyl-glycero-3-phosphocholine (POPC, PC(16:0/18:1)), 1,2-dioleoyl-*sn*-glycero-3-phosphocholine (DOPC, PC(18:1/18:1)), 1-palmitoyl-2-linoleoyl-sn-glycero-3-phosphocholine (PLPC, PC(16:0/18:2)), 1,2-dilinoleoyl-sn-glycero-3-phosphocholine (DLPC, PC(18:2/18:2)), 1-palmitoyl-2-(9′-oxo-nonanoyl)-sn-glycero-3-phosphocholine (PC(16:0/9:0<CHO@C9>)@C9, ALDO PC)), and 1-palmitoyl-2-azelaoyl-sn-glycero-3-phosphocholine (PC(16:0/9:0<COOH@C9>), PAze PC) were purchased from Avanti Polar Lipids (USA). Sodium terephthalate (TA), 2-hydroxy terephthalate (2-HTA) and 4-(*N*,*N*-dimethylaminosulfonyl)-7-(2-aminoethylamino)-2,1,3-benzoxadiazole (DBD-ED) were obtained from TCI Europe (the Netherlands). 13(*S*)-Hydroperoxyoctadeca-9Z,11E-dienoic acid (13-HPODE) was purchased from Cayman Chemical. 2,4-Dinitrophenylhydrazine (DNPH, ≥98%) was ordered from Acros Organics (the Netherlands). Di-4-ANEPPDHQ was ordered from Thermo Fisher Scientific. Triphenylphosphine (TPP), 1-(6-(dimethylamino) naphthalen-2-yl) dodecan-1-one (Laurdan), xylenol orange tetrasodium salt, Ampliflu Red (10-acetyl-3,7-dihydroxyphenoxazine), horseradish peroxidase, valeraldehyde-2,4-DNPH, and 2,2′-dipyridyl disulfide (DPDS) were all ordered from Merck (USA). For all preparations, ultrapure water (Milli-Q-H_2O) was used at 18.2 MΩ cm.

Plasma source

For our experiments, we used the kINPen IND plasma pen as RONS source (Fig. 1 *A*). Inside the plasma jet, a high electric voltage (2–3 kV) is generated by a high-frequency generator (1 MHz) connected to a steel electrode inside a ceramic capillary (18). The vector gas argon flows through the capillary and the high-frequency discharge converts the vector gas into a cold plasma. Argon was used at a flow rate of 4.2 standard liters per minute (slm) and the plasma source operated in the burst mode, which adds a square kilohertz wave (on-off) on top of the megahertz frequency to reduce the production of heat, keeping the plasma at a temperature of ∼40°C. To provide stable and reproducible plasma treatments, the plasma source was switched on at least 20 min before treatment. The treated sample was at a 20° angle to induce constant agitation of the liposome suspension caused by the high vector gas flow. Therefore, the plasma plume generated was not in direct contact with the liposome suspension (Fig. 1 *A*).

Quantification of hydroxyl radical and hydrogen peroxide produced from CAP

Production of hydroxyl (OH·) radical was quantified with TA that is transformed into 2-hydroxyterephthalate (2-HTA) upon reaction with OH·

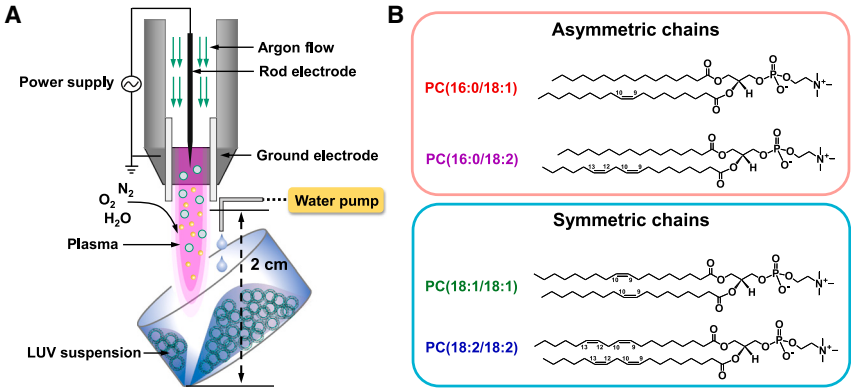

FIGURE 1 Plasma setup and lipids used in this study. (*A*) The plasma source of kINPen IND. One milliliter of LUV suspension is treated with plasma at a distance of 2 cm to prevent the plume touching the suspension. The vector gas stream agitates the suspension evenly during treatment. Milli-Q-H_2O is added into the suspension via a water pump during treatment to compensate for volume loss due to water evaporation. (*B*) Chemical structure of phosphocholine lipids. 1-Palmitoyl-2-oleoyl-*sn*-glycero-3-phosphocholine (PC(16:0/18:1)), 1,2-dioleoyl-*sn*-glycero-3-phosphocholine (PC(18:1/18:1)), 1-palmitoyl-2-linoleoyl-*sn*-glycero-3-phosphocholine (PC(16:0/18:2)), and 1,2-dilinoleoyl-*sn*-glycero-3-phosphocholine (PC(18:2/18:2)).

radicals (19). Specifically, 4 mM TA was added to 1 mL of PBS buffer in glass beaker, and it was placed under plasma plume as indicated in Fig. 1 *A*. After treatment, a certain amount of Milli-Q-H_2O was added back to compensate for water loss during the treatment. 2-HTA was used to make a calibration curve with a concentration ranging from 0 to 100 μM. Excitation and emission wavelength at 310 and 430 nm, respectively, were used to determine the fluorescence of 2-HTA (CLARIOstar reader, BMG LABTECH).

Production of hydrogen peroxide (H_2O_2) from CAP was determined with Ampliflu Red (19). Specifically, 1 mL of PBS buffer was treated with CAP for different times first, and afterward, 2 μM Ampliflu Red and 0.1 U/mL of horseradish peroxidase were added into the treated PBS. Commercial H_2O_2 (Honeywell, 30% (w/w) in H_2O) was used to make the calibration curve. The incubation was kept at room temperature for 20 min. Excitation and emission wavelengths at 563 and 587 nm were used to determine the fluorescence of resorufin (oxidized product of Ampliflu Red by H_2O_2) CLARIOstar reader (BMG LABTECH). Quantities of RONS described in this manuscript reflect cumulative quantities.

Preparation of LUVs

Lipid stock of PC(16:0/18:1), PC(18:1/18:1), PC(16:0/18:2), PC(18:2/18:2), and oxidized lipids, including PC(16:0/9:0<CHO@C9>) and PC(16:0/9:0<COOH@C9>) solutions, were prepared in chloroform. A certain amount of each lipid stock solution was transferred to glass tubes and dried under N_2 stream at room temperature. The solvent was further evaporated by placing the sample in a vacuum desiccator for at least 1 h. The formed lipid film was hydrated with 400 mM KCl solution above transition temperature of each individual lipid for around 30 min. The lipid suspension was then freeze-thawed for at least 10 cycles in dry ice (mixed with ethanol) and a warm water bath (around room temperature). Afterward, the suspension was extruded 10 times by an Avanti Mini-Extruder with filters of 200-nm porosity (Anotop 10, Whatman, Maidstone, UK). The formed LUVs were directly used or stored at 4°C temporarily (maximum 2 days).

K^+ release assay

To test permeabilization of membranes by RONS, we created LUVs that contained 400 mM of KCl in their lumen. For this purpose, the lipid film created in section "preparation of LUVs" was hydrated with 400 mM KCl solution and the formation of LUVs proceeded as described. The formed LUVs were subjected to size-exclusion chromatography to remove K^+ ions outside the LUVs. Specifically, Sephadex G-50 fine (Sigma-Aldrich) gel was hydrated with 400 mM NaCl solution for 2–3 h before being transferred onto a column of 6 mL. This column was further centrifuged for 2 min at 2000 × *g* to remove the water excess and 500 μL of the LUV suspension was slowly added on the top center of the column. The column was then centrifuged at 2000 × *g* for 2 min and the eluate contained the LUVs with a minimal amount of K^+ ions outside the LUVs. The concentration of phospholipids was then determined by phosphorous quantification (20,21).

The collected LUVs were diluted in PBS buffer (Na_2HPO_4/NaH_2PO_4, 50 mM, NaCl 334.8 mM, pH = 7.4), having the same osmolarity as the KCl solution inside the lumen (Fig. S2), to a final concentration of 0.5 mM phospholipids for CAP treatment. One milliliter of each vesicle suspension was treated with CAP for 10, 20, and 40 min. After treatment, 400 μL of this suspension were used to quantify the total amount of K^+ inside and outside the vesicles, and another 500 μL were centrifuged with 30-kDa Amicon Ultra-0.5 Centrifugal Filter for 20 min at 14,000 × *g* to separate LUVs from the released K^+ (filtrate). The percentage of the released [K^+] in the filtrate upon the total [K^+] was then determined by atomic absorption spectroscopy (AAS).

To quantify K^+ by AAS, all samples were first dried at 160°C–180°C and 100 μL of 70% perchloric acid ($HClO_4$) was added into each sample, which was further mineralized at 160°C–180°C for 3 h. Subsequently, 4.8 mL of water and 100 μL of 25% ammonia solution were added to neutralize each sample (final volume was 5 mL). The blanks for AAS consisted of PBS buffer, which was subjected to all operations described for the samples.

A calibration curve was made with stock KCl solution, and its concentration ranged from 0 to 2.5 μg/mL. To account for possible interference from $HClO_4$ and ammonia, we added the same amount of $HClO_4$ and ammonia to each concentration of the calibration curve. The concentration of K was determined by Analytik Jena ZEEnit 700 P AAS Atomic Absorption Spectrometer at 766.4908 nm.

To determine permeabilization kinetics, we fitted K^+ release upon time to an exponential plateau model $K^+_{release}(t) = 100 - (100 - K^+_{release}[t = 0]) * exp(-k * t)$, in which k equals the release rate (min^{-1}) and t is the treatment time. $K^+_{release}(t)$ is the percentage of K^+ at a certain time point t, whereas $K^+_{release}[t = 0]$ indicates the percentage of K^+ release at $t = 0$, respectively. Here, 100 indicates that the maximum possible release percentage is 100%.

Membrane packing quantification

All LUVs were made in 400 mM KCl solution and further diluted in PBS buffer to 0.5 mM phospholipids for CAP treatment. All stock solutions of fluorescent probes were prepared in ethanol and further diluted in PBS buffer. The fluorescence intensity was measured with the CLARIOstar reader (BMG LABTECH) in 96-well plates (Nunc black).

For Laurdan staining, the final concentrations for LUV and probe were 50 μM and 250 nM, respectively. The staining process was conducted at 25°C in the dark for 20 min directly after CAP treatment or 20 h post incubation. The excitation wavelength was 360 nm and emission intensity was scanned from 400 to 600 nm. The generalized polarization (GP) value was calculated from the equation $GP = (I_{440} - I_{490})/(I_{440} + I_{490})$, where I_{440} and I_{490} indicate the fluorescence intensity at 440 and 490 nm, respectively (22).

For di-4-ANEPPDHQ staining, the final concentrations for LUV and probe were 50 μM and 250 nM, respectively. The staining process was conducted at 25°C in the dark for 5 min directly after CAP treatment or 20 h post incubation. The excitation wavelength was 488 nm and an emission scan was obtained from 520 to 740 nm. The GP value was calculated from the equation $GP = (I_{560} - I_{620})/(I_{560} + I_{620})$, where I_{560} and I_{620} correspond to the fluorescence intensity at 560 and 620 nm, respectively (23).

Lipid extraction

For the biochemical analysis of oxidized lipids, all samples were extracted with an improved method based on Bligh and Dyer extraction method (24). Specifically, 1 mL of each LUV suspension was transferred into glass test tubes, and 3.4 mL of Bligh and Dyer solvent mixture (chloroform/methanol/1 M HCl, v/v/v, 10:23:1) was added to each tube. All samples were vortexed for 1 min and placed on ice for 10 min. One milliliter of chloroform and 1 mL of HCl (1 M) were added to each sample. All samples were revortexed for 1 min and incubated on ice for another 10 min. Then, all samples were centrifuged for 5 min at 2000 × *g* and 4°C. The chloroform phase of each sample was taken out and transferred into new glass tubes. One milliliter of chloroform was added to wash the remaining water/methanol phase. Samples were then vortexed and centrifuged for 5 min at 2000 × *g* and 4°C. The first and second chloroform phases were combined and 1 mL of wash buffer (50 mM Tris, 100 mM NaCl, 100 mM EDTA, pH 8.2) was added before the samples were revortexed and recentrifuged in the same conditions as before. The chloroform phase was transferred to a new glass test tube and the remaining water phase was washed again with 1 mL of chloroform. Finally, both chloroform phases were combined, before adding 400 μL of isopropanol and drying the mixture under N_2 gas at ambient temperature. Hereafter, the lipid extracts were dissolved in 500 μL of methanol and extraction efficiency was determined by phosphorous assay.

Analysis with high-performance liquid chromatography/diode array detector -UV-visible/mass spectrometry

A Thermo Finnigan Surveyor system was used for the analysis. A reversed-phase C18 column (Gemini NX-C18 150 × 2 mm × 5 μm, 110 Å; Phenomenex), with a precolumn (Security Guard Gemini NX 4 × 3 mm internal diameter; Phenomenex) was used to analyze the samples and standards at a flow rate of 200 μL/min. Two solvents were used for a gradient separation. Solvent A was 5 mM ammonium acetate in Milli-Q-H_2O:isopropanol (v/v, 75:25) at pH 5.5 and solvent B was isopropanol (high performance liquid chromatography-mass spectrometry (HPLC) grade).

HPLC was coupled to a diode array detector (DAD)-UV-visible (Thermo Finnigan Surveyor DAD) and an electrospray ionization ion source coupled to an ion trap analyzer (LCQ Deca XP plus LC-(ESI)-MS/DAD). This combined detection allowed us to quantify and identify certain oxidized lipids (see quantification of hydroperoxides and lipid aldehydes and ketones below).

All sample and standard vials were kept at 10°C in the HPLC sample holder. Fifty microliters of each sample or standard, together with 50 μL of methanol to fill the rest of the injection loop, was injected for liquid chromatography-mass spectrometry (LC-MS).

Separation of lipid extracts after CAP treatment by HPLC

One-hundred microliters (around 100 nmol) of each lipid extract in methanol was dried with nitrogen stream and redissolved into 200 μL of acetonitrile/H_2O (v/v, 50:50) by vortexing.

The gradient of the mobile phase started at 10% of solvent B, which was held for 4 min. This was followed by an increase of solvent B to 25% over 2 min. From 10 to 18 min, the mobile phase was held at 40% solvent B. In the following 2 min, the percentage of solvent B was increased to 50%, at which percentage it was held for 6 min. Hereafter, the solvent B was increased to 60% in 1.5 min. From 29 to 38 min, the solvent was held at 72% of solvent B. In the following 2 min, solvent B was increased to 100% and was held at this percentage for 3 min. Finally, solvent B was put to 10% from 46 to 55 min to saturate the column for the next analysis.

Quantification of hydroperoxides

13-HPODE was used as a standard to quantify the lipid hydroperoxides formed in polyunsaturated lipid extracts. Stock 13-HPODE was kept in ethanol (stored at −80°C) and further diluted in isopropanol to make a series concentrations ranging from 2.5 to 75 μM. The gradient of mobile phase for standards started at 10% of solvent B, which was held for 3 min. From 6 to 10 min, the mobile phase was held at 40% solvent B. In the after 2 min the percentage of solvent B was increased to 100%, at which percentage it was held for 3 min. From 17 to 25 min, solvent B was held at 10% for the next analysis.

Although a UV detector at 234 nm was used to quantify the hydroperoxides derived from polyunsaturated lipids (25), mass spectrometry was used in parallel to determine their structure. The DAD scanned a wavelength range from 190 to 400 nm to discern hydroperoxides with a maximum at 234 nm from other oxidation products. Mass spectra were recorded in both the negative and positive ion mode at a range from 150 to 2000 m/z to identify the corresponding structures.

To quantify the total amount of hydroperoxides, ferrous oxidation-xylenol orange (FOX) assay was used (26). Briefly, 200 μL of FOX reagent and 20 μL of lipid extract were mixed and incubated for around 20 min at room temperature. Finally, the absorbance of all samples was measured at 580 nm and H_2O_2 was used to make a calibration curve.

Quantification of aldehydes and ketones

Valeraldehyde-2,4-DNPH was used as a standard to quantify the DNPH signal. Stock valeraldehyde-2,4-DNPH was dissolved in acetonitrile (stored at 4°C) and was further diluted in acetonitrile/H_2O (v/v, 50:50) to make a series concentrations ranging from 0.5 to 50 μM. The gradient of mobile phase for standards started at 25% of solvent B, which was held for 3 min. From 6 to 10 min, the mobile phase was held at 40% solvent B. In the after 2 min, the percentage of solvent B was increased to 100%, at which percentage it was held for 3 min. From 17 to 25 min, solvent B was held at 25% for the next analysis.

Derivatization of aldehydes with 2,4-DNPH in combination with HPLC-DAD-MS was used to quantify their production. Specifically, 12 mM stock DNPH reagent was made by dissolving DNPH in acetonitrile in the presence of 2% formic acid (27). One-hundred microliters of lipid extract (around 100 nmol) were dried under N_2 stream before 100 μL of stock DNPH reagent and 100 μL of water were added. All samples were rigorously vortexed and kept at room temperature in the dark for 2 h. Then the samples were transferred to autosampler vials for LC-MS analysis. Valeraldehyde-2,4-DNPH (Sigma-Aldrich) was used as standard to make a calibration. Limit of detection (LOD) and limit of quantification (LOQ) were determined by the standard curve (Table S2). We derivatized a known amount of 16:0-9:0 (ALDO) PC (1-palmitoyl-2-(9′-oxo-nonanoyl)-sn-glycero-3-phosphocholine) to evaluate the reaction efficiency. Combining mass detection (m/z) and UV absorbance at 364 nm permitted us to identify and quantify derivatized lipid aldehydes.

Quantification of lipid carboxylic acids

Derivatization of carboxylic acids was done with 4-(*N*,*N*-dimethylaminosulfonyl)-7-(2-aminoethylamino)-2,1,3-benzoxadiazole (DBD-ED) in the

presence of triphenylphosphine (TPP) and DPDS to quantify their amount in treated samples (28). Specifically, stock solutions of 5 mM DBD-ED, 28 mM TPP, and 28 mM DPDS were prepared in acetonitrile. One-hundred microliters of lipid extract (around 100 nmol) were first dried and then redissolved in 50 μL of isopropanol into which 50 μL of each stock solution (DBD-ED, TPP, and DPDS) were added. All samples were vigorously vortexed and incubated for 2 h in the dark at room temperature. Afterward, 10 μL of each sample together with the standards were spotted on a normal phase silica TLC plate using the CAMAG Linomat 5 (CAMAG, Wilmington, NC, USA). As external standard we used 1-palmitoyl-2-azelaoyl-sn-glycero-3-phosphocholine (PC(16:0/9:0<COOH@C9>), PAzePC, from Avanti Polar Lipids) which was derivatized in the same conditions to make a calibration curve from 0.025 to 0.75 nmol. The mobile phase to develop the TLC plate was a mixture of chloroform/methanol/water/25% ammonia (v/v/v/v, 30:20:2:1). The image of the TLC plate was scanned with the GelDoc Go Imaging System (Bio-Rad) UV tray using the program for SYBR Green stain. LOD and LOQ were determined by the standard curve (Table S2).

Semi-quantitative determination of oxidized lipids with various oxygen atoms

In addition to the fully quantitative analyses described above, we used a semi-quantitative method to determine oxidized lipids with different numbers of oxygen atoms such as hydroxyls or ketones. A full quantitative approach of these substances is difficult because of missing standards for the huge variety of oxidized lipids. The relative amount of oxidized lipids was expressed as the percentage of the corresponding peak area upon the peak area of the original lipid (corresponding host lipid that was not oxidized in the same sample). Mass spectrometry analysis was done in the negative ionization mode (29). We used the LPPtiger nomenclature in this manuscript to avoid confusion of oxidized species (30).

Surface tension determination with pendant-drop tensiometry

Surface tension of PBS buffer with or without LUVs was determined. For PBS with LUVs, all LUVs were made in 400 mM KCl solution and further diluted in PBS buffer to a final concentration at 0.5 mM before being treated by CAP for 40 min. LUVs without any treatment were used as negative controls. The positive controls were made by adding 0.1% Triton X-100 to the LUV suspension. For PBS without LUVs, PBS buffer alone was treated with CAP for 40 min. PBS buffer without any treatment was used as PBS control. Positive control was obtained by adding 0.1% Triton X-100 to PBS buffer. Surface tension of direct effects was determined directly after treatment, and 20-h post-incubation effects indicated the surface tension was determined after 20 h (at room temperature) after being treated by 40 min CAP or 0.1% Triton X-100.

Measurements of interfacial tension between air and liquid were carried out using a pendant-drop tensiometer (DataPhysics OCA) by fitting the droplet shape with the Young-Laplace equation. The liquid drop was dispensed with a 1-mL syringe together with an OKI TE needle 20G (METCAL).

Dynamic light scattering analysis

LUV sizes and distribution were analyzed by dynamic light scattering (DLS) with a Malvern Zetasizer Nano-ZS at an angle of 173° for backscattering detection. All measurements were conducted at 25°C.

Statistical analysis and principal-component analysis

Statistical analyses were performed using GraphPad Prism version 9.3.1. Data were obtained from at least two independent experiments ($n = 2$) and multiple repeats unless stated. The comparative statistical analysis between conditions were carried out using one-way ANOVA and two-way ANOVA comparison tests. Principal-component analysis (PCA) was done in Rstudio (2022.07.01, build 554) with R (v. 4.2.1.) using the ggbiplot plugin.

RESULTS

RONS production by kINPen IND

To produce RONS, we used the kINPen, which is a plasma pen that has been optimized to produce a large amount of OH· radicals (31). In our setup (Fig. 1 *A*), the generated plasma plume does not touch the liquid suspension that contains the membrane models (LUVs). The electric field will not interfere in vesicle permeation because it is too weak outside the plume, meaning that permeabilization or other changes of membrane properties will be induced by lipid oxidation. We first assessed the quantity of RONS that were produced in our setup by determining the amount of OH• radicals and H_2O_2 at the corresponding incubation times (Fig. S1 *A* and *B*). Although OH• radicals were detected at micromolar range, H_2O_2 reached millimolar levels at 20 min of CAP treatment. Since the quantity of RONS that is produced in the chosen condition is reproducible, we assume that main differences on membrane effects resulted from initial lipid compositions.

Permeabilization by RONS is mediated via two different mechanisms

K^+ ions play important roles in many cellular processes (32), especially in membrane potential maintenance. The lipid bilayer of cell membranes is generally not permeable toward K^+, with the concentration gradient between the cytoplasm and exoplasm being mainly maintained by the Na^+/K^+-ATPase pump. Here, we quantified K^+ leakage in LUVs made of phosphatidylcholine lipids with different symmetric or asymmetric combinations of mono- and polyunsaturated acyl chains by AAS directly upon CAP treatment and after a 20-h post-incubation period at ambient temperature.

We started out with several control experiments to rule out factors that could potentially influence membrane permeability or lipid oxidation. First, a difference in osmotic pressure between the inside and the outside of vesicles may favor permeabilization of LUVs. Since CAP induces the formation of new species, we might observe a significant increase of osmolarity outside of vesicles. However, during all our setups, no significant change of osmolarity could be observed during treatment, ruling out this possibility (Fig. S2 *A*). As described earlier, the effect of the generated electric field and hence electro permeabilization can also be ruled out in our current setup. Furthermore, acidity is an important factor that could influence lipid oxidation. However, the pH remained unaffected in our setup, excluding related effects (Fig. S2 *B*).

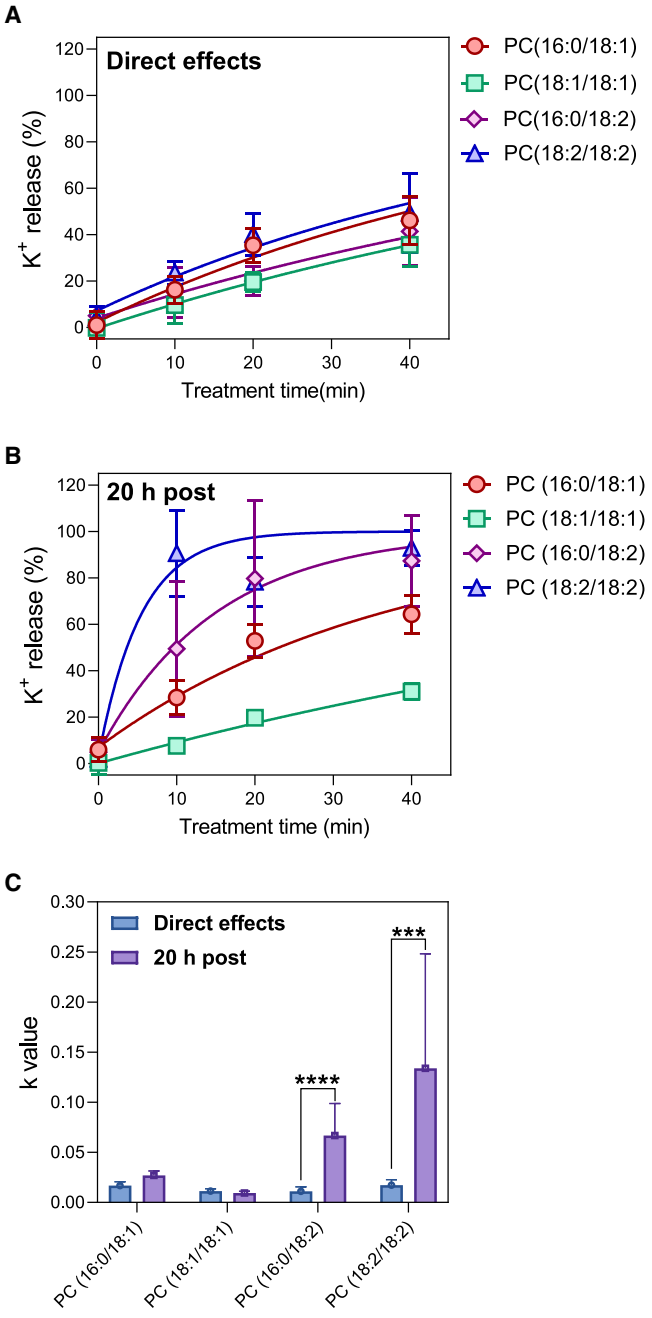

FIGURE 2 Permeabilization kinetics, characterized via K^+ release, are drastically altered upon post-incubation. K^+ release in percentage of LUVs made with PC(16:0/18:1) (*red circles*), PC(18:1/18:1) (*green squares*), PC(16:0/18:2) (*purple diamonds*), and PC(18:2/18:2) (*blue triangles*) induced by CAP after (*A*) direct treatment and (*B*) 20-h post-incubation. (*C*) Rate constant (***k***) of membrane permeabilization according to an exponential plateau model described in section "materials and methods." One-way ANOVA analysis was used to compare ***k*** values between direct effects and 20-h post-effects for all LUVs, respectively. The curves represent an average from at least two independent experiments done in triplicate ($n \geq 6$, *p < 0.05, **p < 0.01, ***p < 0.001, ****p < 0.0001). Error bars correspond to standard deviation.

As shown in Fig. 2 *A*, CAP induced a gradual K^+ release from LUVs during a 10- to 40-min treatment period. The rate of K^+ release (***k*** value) in these four different LUV compositions does not appear to vary significantly during the 10- to 40-min treatment period, indicating that unsaturations do not sensitize membranes toward direct RONS damage (Fig. 2 *C*). By contrast, after a 20-h post-CAP treatment period, the amount of K^+ release increased particularly in polyunsaturated PC lipids (i.e., PC(16:0/18:2) and PC(18:2/18:2)) (Fig. 2 *B*) with the ***k*** value related to the rate of release increasing only in LUVs made of polyunsaturated lipids (Fig. 2 *C*). These results indicate two different release mechanisms, one independent of unsaturation and another depending strongly on unsaturation. Curiously, we observed that K^+-release was always higher in PC(16:0/18:1) LUVs than in PC(18:1/18:1) LUVs, suggesting that oxidized lipid species of asymmetrically monounsaturated lipids might be more powerful in permeabilizing the membrane.

Membrane packing alterations by RONS depend on lipid unsaturations

Packing of lipid membranes is an important biophysical property that is related to many functional aspects of membranes, such as permeability and lateral diffusion of lipids and proteins. Modulation of membrane packing through external or internal stimuli can have large consequences for the evoked functions and can lead to the impairment of membrane signaling and cell death in absence of adaptation (33,34). To examine whether CAP alters membrane packing, we applied two environmental polarity sensitive dyes, Laurdan and di-4-ANEPPDHQ, which have been widely used to quantify membrane packing in both model membranes and living cells (35,36). In principle, di-4-ANEPPDHQ probes only the outer leaflet of the membrane bilayer due to its positive charges and hence incapacity to flip to the inner leaflet (37). If damage occurs only to the outer leaflet, this probe should be more sensitive than Laurdan. Further, the fluorophore of di-4-ANEPPDHQ is assumed to probe polarity close to the headgroup/water interface (38). Laurdan probes the polarity of both membrane bilayer leaflets in between acyl chains and lipid headgroups (39,40), hence at a slightly deeper location in the membrane bilayer than di-4-ANEPPDHQ.

We observed that oxidation induced a slight increase of Laurdan GP in all LUVs after 40 min of CAP treatment, indicating either that fewer water molecules are in the vicinity of Laurdan and packing has increased, or the polarity of its microenvironment has decreased (Fig. 3 *A*). After 20 h of post-incubation, we observed a large increase of Laurdan GP only in polyunsaturated lipids (Fig. 3 *A*), similar to the strong increase of permeabilization (Fig. 2 *B*). Changes of similar magnitude appeared measuring di-4-ANEPPDHQ GP, but, surprisingly, in the opposite direction, with a decrease of GP, indicating less packing or an increase of the polarity in the microenvironment (Fig. 3 *B*). These opposite trends could arise from the fact that CAP induces

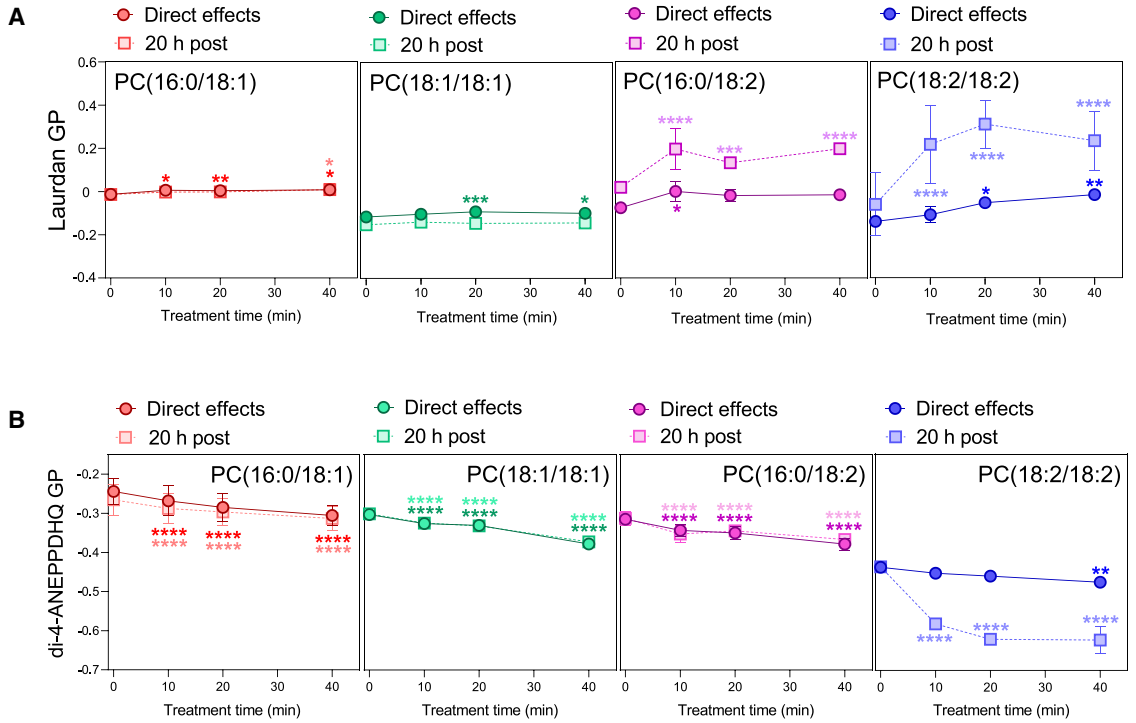

FIGURE 3 Laurdan (*A*) and di-4-ANEPPDHQ GP (*B*) are altered differently upon CAP treatment, whereas the largest changes are observed in polyunsaturated lipids upon 20-h post-incubation. Effect on GP upon direct CAP treatment (*dotted darker line*) and 20-h post-incubation (*dashed lighter line*) in different LUV suspensions. Two-way ANOVA analysis was used to compare the differences in GP after treatment toward the corresponding negative controls. The GP values were from the average of at least two independent experiments, done in triplicate ($n \geq 6$, *p < 0.05, **p < 0.01, ***p < 0.001, ****p < 0.0001). Error bars correspond to standard deviation.

differential changes upon membrane depth, which might be explained by the large variety of oxidized species being formed (see below). A somehow compensatory effect might also explain the absence of large packing changes probed by di-4-ANEPPDHQ on PC(16:0/18:2) after post-incubation.

Quantification of oxidized phosphatidylcholines

Production and diversity of hydroperoxides

To examine the complex relationship of permeabilization or membrane packing with the formation of oxidized phosphatidylcholines (OxPCs), we quantified and characterized the formation of OxPCs upon incubation of LUVs with RONS, generated by CAP. For the quantification of total hydroperoxides in LUVs, the FOX assay was used (Fig. 4 *A*) (26,41,42). In PC(16:0/18:2) and PC(18:2/18:2) LUVs, lipid hydroperoxides were further quantified by HPLC-UV-MS, taking advantage of the specific UV absorbance of conjugated dienes at 234 nm (Fig. S3). A comparison of both methods revealed an equal specificity toward hydroperoxides, albeit that the FOX assay gives higher values because it determines the amount of all –OOH functions in the lipid extract, whereas the LC-UV method determines the amount of individual –OOH lipids. We observed that RONS produced by CAP induced detectable amounts of lipid hydroperoxides only in LUVs made of polyunsaturated lipids (e.g., PC(16:0/18:2) and PC(18:2/18:2)) (Figs. 4 *A* and S3). Twenty hours of post-incubation led to a huge increase of hydroperoxides in these LUVs, especially in PC(18:2/18:2), indicating a strong dependence on the number of unsaturations.

The distribution of hydroperoxide species in PC(16:0/18:2) and PC(18:2/18:2) LUVs is summarized in Fig. 5 *A* and *B*. The complexity and diversity of lipid hydroperoxides rose upon increasing numbers of unsaturated double bonds (Figs. 5 *A* and *B* and S3). Hydroperoxides with one –OOH were the most abundant in both PC(16:0/18:2) and PC(18:2/18:2) LUVs, followed by those with two –OOH or three –OOH functional groups.

Production and diversity of OxPCs with truncated acyl chains

Next, we focused on lipid oxides with truncated acyl chains, including lipid aldehydes and carboxylic acids that can be produced from the decomposition of lipid hydroperoxides at the unsaturation sites via Hock rearrangement or the formation of a dioxetane (43,44). DNPH derivatization in combination with LC-MS-UV was used to quantify truncated and nontruncated aldehydes and ketones (27). Truncated phospholipids with aldehyde and ketone groups were by far the most common products, whereas ketone addition products were only obtained in significant amounts in polyunsaturated lipids (~10% in PC (16:0/18:2) and 10%–20%

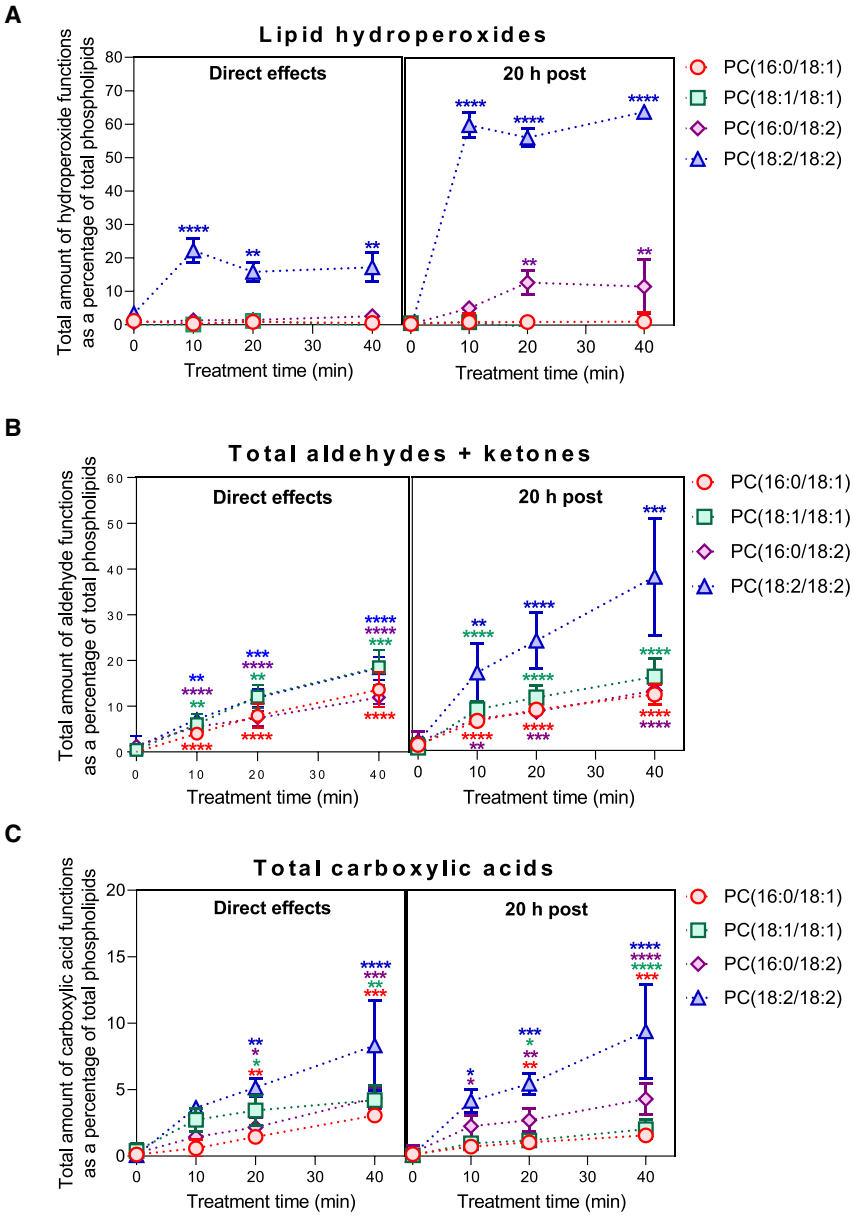

FIGURE 4 Production of oxidized products in LUVs containing lipids with different degrees of unsaturations, induced by CAP directly after treatment (*left panels*) and 20-h post incubation (*right panels*) expressed as percentage of total phospholipids. (*A*) Total amount of hydroperoxide functional groups, (*B*) total amount of aldehyde and ketone functional groups, and (*C*) total amount of carboxylic acid functional groups as a percentage of total phospholipids. The total amount of hydroperoxide functional groups were determined by FOX assay (see section "materials and methods"). Two-way ANOVA analysis was used to compare the difference between CAP-treated samples and corresponding negative control for both direct treatment and 20-h post-incubation respectively. At least two independent experiments in duplicate were performed for each assay ($n \geq 4$, *p $<$ 0.05, **p $<$ 0.01, ***p $<$ 0.001, ****p $<$ 0.0001). Error bars correspond to standard deviation.

in PC (18:2/18:2) out of their corresponding total DNPH signal) (Fig. 5 *E* and *F*). In PC (18:2/18:2), a small amount of DNPH peak area (5%–10%) after 20 h of post-incubation contained truncated lipids and addition products, which made it impossible to assign this quantity to any of the products (Fig. 5 *F*). Interestingly, we observed that the total amount of aldehydes and ketones was similar in lipids with symmetrically unsaturated acyl chains (PC(18:1/18:1) and PC(18:2/18:2)) and significantly higher compared to asymmetrically unsaturated acyl chains (PC(16:0/18:1) and PC(16:0/18:2)) directly after CAP treatment (Figs. 1 and 4 *B*). This implies that production of these species depends on the number of unsaturated acyl chains, rather than the total number of lipid unsaturations. Noticeably, 20-h post-incubation only resulted in further accumulation of these species in PC(18:2/18:2) LUVs, and this seemed mainly due to the accumulation of ketone addition products.

Conversely to the amount of lipid aldehydes, the diversity of aldehyde species increased upon the total number of unsaturations. The variety of species is summarized in supplementary tables (Supplemental data files S1–S4).

In addition to aldehydes, lipid carboxylic acids constitute the most common truncated OxPCs. Lipid carboxylic acids derive from either the oxidation of lipid aldehydes or the decomposition of secondary oxidized products (e.g., lipid hydroperoxides, ketones, hydroxides, and ozonides) (45). The total amount of lipid carboxylic acids seemed to be positively correlated with the total number of unsaturated

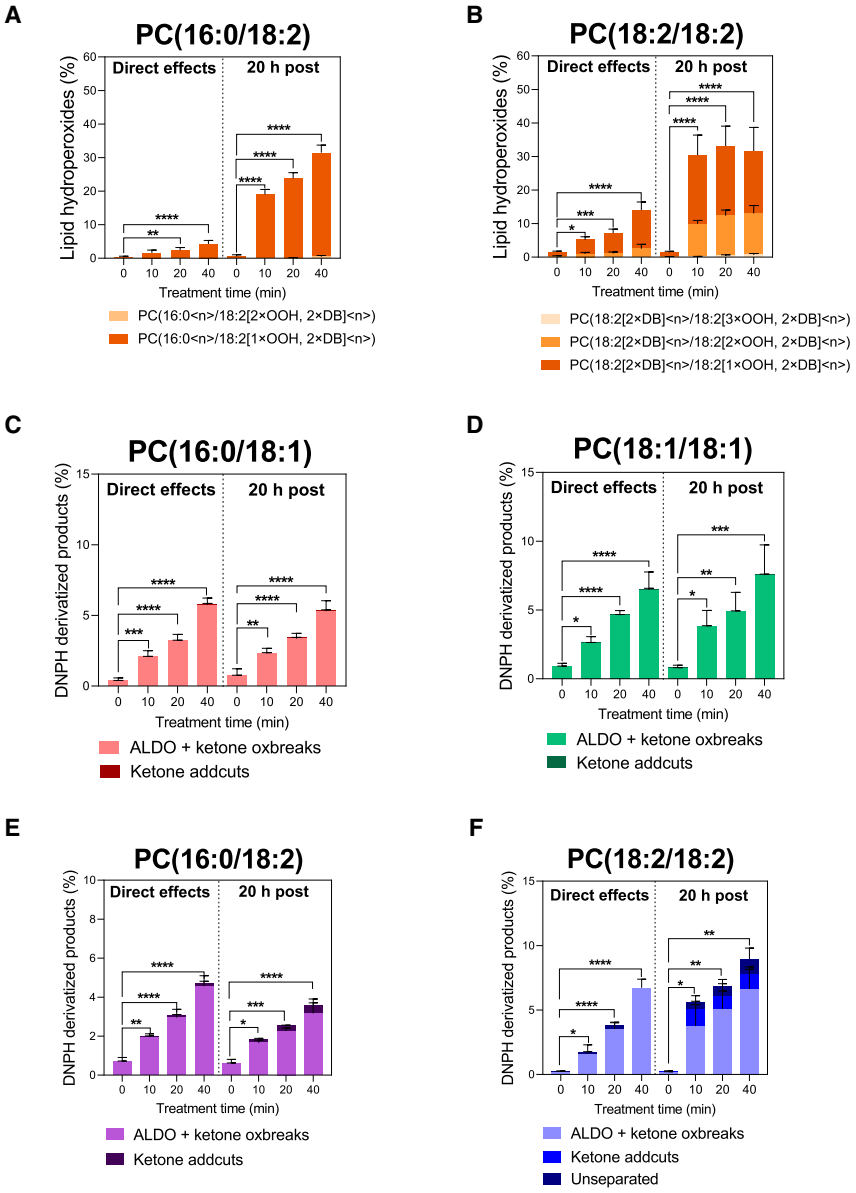

FIGURE 5 Production and diversity of individual lipid hydroperoxides and lipid aldehydes and/or ketones induced by CAP. Production and diversity of lipid hydroperoxides in (*A*) PC(16:0/18:2) and (*B*) PC(18:2/18:2) LUVs induced by CAP after direct treatment and 20-h post-incubation. Distribution of oxidatively truncated lipid aldehydes and ketones (ALDO + ketone oxbreaks), ketone oxygen addition products (ketone adducts), or DNPH signal originating from peaks that contain both types of products (unseparated) out of total DNPH signal in (*C*) PC(16:0/18:1), (*D*) PC(18:1/18:1), (*E*) PC(16:0/18:2), and (*F*) PC (18:2/18:2) directly after CAP treatment and 20-h post-incubation. The proposed structures of lipid aldehydes and ketones are presented in supplementary files (Supplemental data files S1–S4). Two-way ANOVA analysis was used to compare the difference between CAP-treated samples and corresponding negative control for both direct treatment and 20-h post-incubation, respectively. At least two independent experiments were performed in duplicate for the quantification hydroperoxides, aldehydes, and/or ketones ($n \geq 4$, *p $<$ 0.05, **p $<$ 0.01, ***p $<$ 0.001, ****p $<$ 0.0001). Error bars correspond to standard deviation.

double bonds and post-incubation induced only slight changes (Fig. 4 *C*).

Production and diversity of other OxPCs

Lipid hydroxyls, ketones, or epoxides can be formed by either rearrangement of lipid hydroperoxides or direct formation by reacting with hydroxyl radicals (46,47). Moreover, ozone (O_3), which is also produced by CAP, reacts with unsaturated lipids as well, resulting in ozonides (48,49). Considering the lack of standardized quantitative approaches for the determination of these oxidized lipid species (except ketones, Fig. 5 *C–F*), and their relatively small amount, we applied a semi-quantitative approach (29) by presenting the distribution of OxPCs with different numbers of oxygen atoms in Fig. S4. We observed that more oxygen atoms were added to host lipids upon CAP treatment time and post-incubation, and that this trend also depended on unsaturations (i.e., polyunsaturated LUVs have ∼10 times more addition of oxygen than monounsaturated LUVs). We further observed that the largest relative peak area could be related to the formation of hydroperoxides, especially in polyunsaturated lipids (Fig. S4, *OO).

OxPCs are released from host LUV bilayer

To investigate whether OxPCs remain in the membrane of host LUVs, or whether they escape the membrane and adsorb at the air-water interface, we measured the surface tension after various treatment conditions. In this "pendant-drop" experiment, a drop is formed instantly,

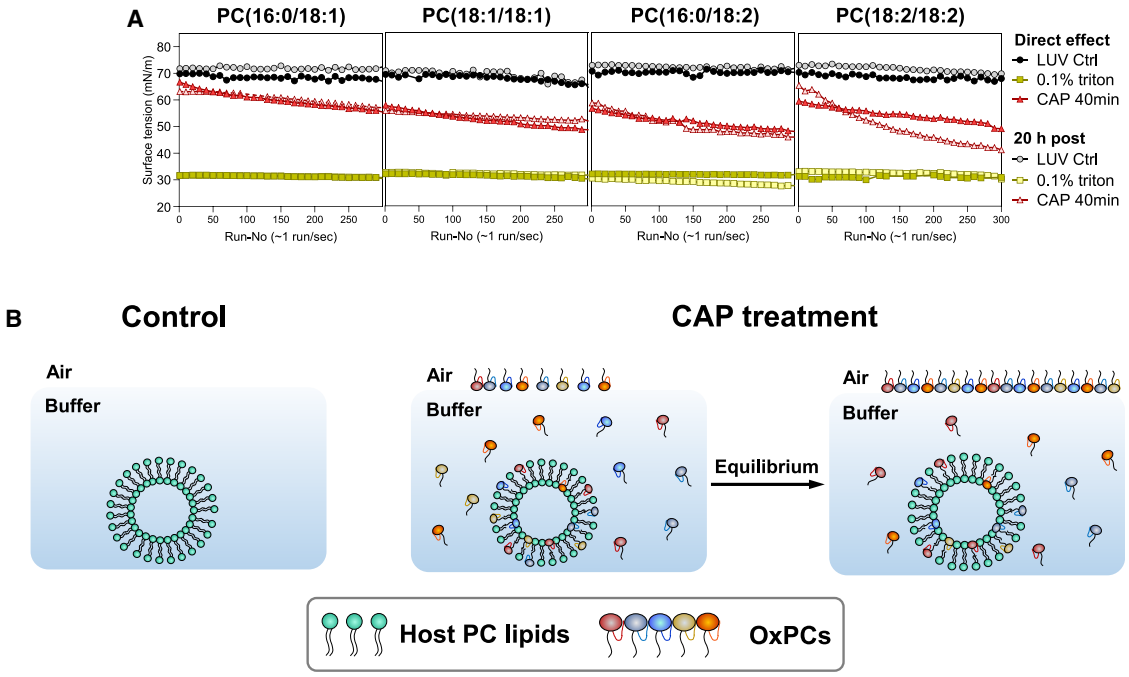

FIGURE 6 Interfacial tension determination with pendant-drop tensiometry. (*A*) Interfacial tension of PBS buffer containing LUVs either directly after CAP treatment or after 20-h post-incubation; 0.1% Triton X-100 was used as positive controls. (*B*) Proposed process of interfacial tension reduction induced by OxPCs in all above LUVs. Since PC lipids tend to form lipid bilayers, in negative control (LUV Ctrl), there are no free lipids in solution or micelle formation on the timescale of the experiment. When a certain amount of OxPCs is formed, some OxPCs are released from lipid bilayers due to the increased hydrophilicity. Afterward, those released OxPCs adsorb at the buffer-air interface, resulting in a reduction of surface tension. Two independent experiments were performed for interfacial tension measurements and averages are displayed in the curves.

and directly hereafter amphiphilic substances can adsorb at the air-water interface upon the timescale of the experiment (Fig. 6). A reduction in surface tension is hence induced by the adsorption of amphiphilic molecules (e.g., surfactants) at the water-air interface. For LUV controls without CAP treatment (Fig. 6 *A*), no significant decrease in surface tension was observed within the observation timescale, regardless of the number of unsaturations, meaning there was no release of phospholipids into the air-water interface on the timescale of the experiment. Triton X-100, a known surfactant, effectively reduced surface tension in buffer (Fig. S5 *A*) and LUV suspensions (Fig. 6 *A*), showing its potency in adsorbing at the water-air interface.

CAP treatment reduced surface tension in all LUV suspensions (Fig. 6 *A*) but not of pure PBS buffer, indicating that RONS on their own have no effect on surface tension reduction, but oxidized lipids do (Fig. S5 *B*). Post-incubation caused a slightly larger reduction of this interfacial tension only in LUVs made of PC(18:2/18:2). Our results indicate that certain OxPCs are released from the host LUV membrane bilayer and adsorb at the air-water interface, thereby reducing surface tension (Fig. 6 *B*) (50,51).

Interestingly, DLS analysis shows neither a significant reduction in average size for all treated LUVs nor the formation of small aggregates such as micelles (Fig. S6 *A–D*). This could mean that only a small amount of the formed OxPCs is released from the host LUV membrane bilayer into the aqueous phase, the air-water interface. Another possibility is that the reduction of size of LUVs due to the release of certain oxidized lipids is compensated by the formation of molecules with a larger molecular surface than the original phospholipids such as lipid hydroperoxides (17).

Lipid oxidation increases the polarity of lipids, especially if oxidation leads to truncation of an acyl chain, such as during the formation of aldehydes or carboxylic acids (Table S1). According to the prediction of logP (Table S1), the effective partitioning into the aqueous phase should increase by a factor of $\sim 10^2$ if an oxygen atom is added to the acyl chains and by a factor of $\sim 10^5$ if the chain is oxidatively truncated. The chances are hence large that truncated phospholipids can effectively partition into the aqueous phase.

Interestingly, the rate by which the surface tension is decreased depends strongly on the structure of the oxidized lipid (Fig. S5 *B*) and is different for post-incubation in PC(18:2/18:2) (Fig. 6 *A*). The residence time of a lipid in a bilayer is commonly defined as $\tau_R = \tau_0 / e^{-\Delta E/kT}$ where τ_R is the mean residence time in s^{-1}, τ_0 is the motional correlation time for amphiphiles in bilayers ($\sim 10^{-7}$ s), ΔE is the activation energy for the lipid to escape the bilayer, k is the Boltzmann constant, and T the temperature in Kelvin. This expression can be approximated by $\tau_R \approx 55\tau_0/CMC$, where CMC is the critical micellar concentration of the lipid (or critical aggregation concentration for bilayer forming

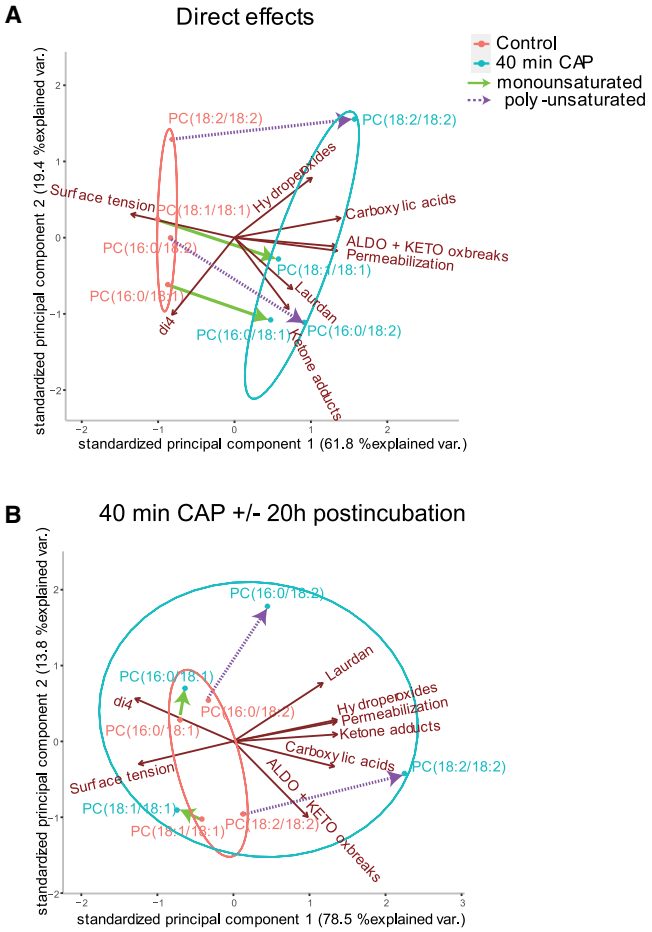

FIGURE 7 PCA displaying the development of average membrane properties and surface tension in parallel to the formation of specific OxLipids (*brown arrows*). (*A*) Untreated (*red group*) vs. 40-min CAP treatment (*blue group*), and (*B*) 40-min CAP treatment without (*red group*) vs. with 20-h post-incubation (*blue group*). Modifications of properties from individual LUV samples are highlighted by green (monounsaturated lipids) and purple arrows (polyunsaturated lipids).

lipids). From the measured CMC/CAC of phospholipids, the escape rate should increase by a factor of 4–10 if two CH_2 groups are "cut off" the lipid (52,53). From these theoretical considerations, it seems that truncated lipids are the best candidates to be most quickly released from the bilayer and hence reduce surface tension.

PCA of membrane properties and lipid oxidation

A PCA reveals the connection of different parameters in treated samples by visualizing variations of multiple parameters into a two-dimensional space. In our analysis, the directions of brown arrows indicate the development of parameters such as permeability. (Fig. 7). If arrows are almost parallel, parameters are positively correlated and evolve into similar directions (increase or decrease) upon samples (LUVs) and conditions (control, CAP treatment, post-incubation). If the arrows point in opposite directions, the parameters are negatively correlated, meaning that, if one parameter increases, the other decreases or vice versa. Conversely, if arrows are perpendicular, then these parameters are probably not correlated. LUV samples that are close on the PCA coordinate system have similar properties.

The most informative PCAs were obtained comparing control samples vs. 40-min-treated CAP samples without post-incubation (Fig. 7 *A*), and 40 min CAP treatment without post-incubation vs. 40-min CAP treatment with 20-h post-incubation (Fig. 7 *B*).

PCA revealed that all LUV samples evolved in similar directions on the PCA plane upon direct CAP treatment, meaning that oxidation of lipids, permeabilization, and packing developed similarly for all samples, regardless of lipid unsaturations (Fig. 7 *A*, green and purple arrows). We observed further that permeabilization was closely linked to the formation of truncated aldehydes and ketones, and slightly less to carboxylic acids, whereas hydroperoxides and ketone adducts seemed less correlated to this trend (Fig. 7 *A*, brown arrows). This means that hydroperoxides and ketone adducts play a minor role in the permeabilization mechanisms for direct treatment, which is supported by the fact that no hydroperoxide and almost no ketone adduct is formed for monounsaturated lipids, although permeabilization is progressing (Figs. 2 *A*, 4 *A*, 5 *C* and *D*). Interestingly, surface tension evolved in the opposite direction of especially truncated aldehydes and ketones, and carboxylic acids, meaning that surface tension decreased upon formation of especially truncated oxidized phospholipids (Fig. 7 *A*).

Comparison of samples treated for 40 min and that were either submitted to 20-h post-incubation or not provided a different picture. Sample points of polyunsaturated lipids (purple arrows) evolved strongly on the PCA plane (large distances), whereas differences for monounsaturated lipids remained small (green arrows) (Fig. 7 *B*). This means that post-incubation affects mainly LUVs of polyunsaturated lipids. Changes to permeabilization, due solely to post-incubation, were less linked to the formation of truncated lipids but rather to hydroperoxide and ketone adducts formation (Fig. 7 *B*, brown arrows). It appears, though, that long-term permeabilization might be promoted by oxygen addition products such as hydroperoxides. This implies that permeabilization proceeds possibly via two different mechanisms, one that is quite rapid and depends on acyl chain breaking and another that depends on longer post-incubation periods and the formation of oxygen addition products. Surface tension here was also rather linked to the formation of hydroperoxides and ketone adducts, meaning that their release to the aqueous environment or the air-water interface is slower, as discussed before (Fig. 7 *A* and *B*).

The picture for packing investigated by di-4-ANEPPDHQ and Laurdan GP is less clear, although large changes in GP appear only upon the formation of oxygen addition products (Figs. 3 *A* and *B* and 7 *B*).

It is, unfortunately, not certain how other lipid oxides such as hydroxyls, epoxides, or ozonides might contribute to changes of membrane properties since we did not quantify them in an absolute manner (Fig. S4). However, the relative increase of these peaks in LC-MS is very small compared to the formation of truncated oxidized phospholipids or ketone addition products plus hydroperoxides, especially in polyunsaturated lipids (Fig. S4), suggesting that the quantified oxidized lipids should be responsible for the main effects observed.

DISCUSSION

Lipid peroxidation is ubiquitous but the modulation of different biophysical properties of the membrane upon formation of oxidized lipids is still poorly understood because of the huge complexity of possible oxidation products in biological and even model membranes. By using model membranes made of mono- and polyunsaturated lipids with one unsaturated (asymmetric) or two unsaturated (symmetric) acyl chains, we analyzed how structural properties of lipids guide the alteration process of membranes upon oxidation and identified the main oxidized lipid species that are responsible.

Our data, combined with PCA, suggest that two different permeabilization mechanisms exist. The first mechanism leads to rapid permeabilization parallel to the formation of truncated lipids, in mono- and polyunsaturated lipids. Hence, the associated oxidative cleavage does not depend on the unsaturation degree if at least one unsaturation is present. The formation of cleaved lipid aldehydes and carboxylic acids can happen via formation of hydroperoxide intermediates and subsequent Hock cleavage or dioxetane formation (54). This mechanism is based on hydrogen abstraction from the C_α carbon of the acyl chain. Another mechanism to produce truncated lipids is based on the formation of Criegee ozonides, which requires the formation of ozone, produced by the CAP source (55,56). Since there are almost no hydroperoxides present in the monounsaturated models, oxidative cleavage might not rely on the intermediate of hydroperoxides here, except if they are very unstable in the present conditions. The kINPen produces a cold plasma containing a large variety of RONS; thus, it is difficult to say which oxidation mechanism is dominating. We can assume that short-living reactive species ($OH\cdot$, $OOH\cdot$, O, O_3, O^{2-}, $^1O_2$) play a major role here since they can induce fast hydrogen abstraction and subsequent acyl chain truncation. The kINPen is known to generate large amounts of $OH\cdot$ radicals, as determined in Fig. S1, thus these might be the main species inducing short-term damage (18). It was shown earlier that indirect treatment by plasma does not induce direct permeabilization, excluding a significant effect of long-living RONS (57).

It has been proposed in other studies that truncated lipids are the driving factor for membrane permeabilization (12,13,58–60). Generally, an increase of positive intrinsic molecular curvature due to truncation of the acyl chains goes along with an increase of polarity of the side chain due to aldehyde or carboxylic acid formation (Table S1). This parallel increase of membrane polarity and the amount of positively curved lipids could lead to the formation of toroidal pores at a certain threshold of oxidized lipids (13,61). The truncated lipids, or their short-chain oxidized counterparts, are probably also responsible for the observed reduction of surface tension, as discussed before. Since there is no decrease of LUV size, chances are real that the amount of released lipids is small, especially since no hydroperoxides with a high molecular surface area are formed in LUVs of monounsaturated lipids that could compensate for the area change.

The continuous K^+ release observed during this "fast" mechanism could be explained by 1) the formation of short-living "membrane instabilities" that are associated with the instant formation of truncated lipids by short-living RONS, 2) formation of toroidal pores that are only formed at a certain threshold concentration of truncated lipids and that are inhibited by the constant release of pore forming OxPCs from the membrane, or 3) the asymmetric oxidation of both monolayers. In our case, the formation of truncated lipids in the outer monolayer could create a concentration gradient, forcing the flipping of these oxidized lipids to the inner leaflet and thereby creating possible transient instabilities. Preferential oxidation of the outer monolayer has been proposed as a mechanism in giant unilamellar vesicle membrane destabilization (60).

The second permeabilization mechanism is only observed during long-term incubation of polyunsaturated lipids. Since only hydroperoxides increased strongly in LUVs with polyunsaturated lipids upon post-incubation, we suspect that this "slow" permeabilization is based on hydroperoxide formation, even though other addition products, such as ketones, might play a role. Interestingly, this permeabilization is coupled to a huge increase in Laurdan GP. This increase in packing or reduction of the water incursion might be due to the increase in surface area per molecule that is predicted upon formation of hydroperoxides. Formation of hydroperoxides might also induce a lateral rearrangement of other oxidized lipids in the membrane. It has been shown that hydroperoxides are able to phase separate from other lipids (17,62), meaning that the effective surface for other oxidized lipids, such as aldehydes or carboxylic acids, on an LUV could be reduced, which would increase their local concentration and hence their efficiency in permeabilizing membranes. If hydroperoxides are mainly created on the outer monolayer, the area increase of the outer monolayer could create an area difference between inner and outer leaflet and thereby promote membrane instabilities (60). Effects related to area difference should, in theory, be compensated by quickly flip-flopping lipids such as cholesterol, which is not present in our models.

A threshold for permeabilization by oxidized lipids was proposed by several authors (12,63). Runas et al. observed a large increase of passive diffusion of an uncharged molecule from 2.5% to 10% POxnoPC (i.e., PC(16:0/9:0<CHO@C9>)). At this concentration of oxidized lipid, no diffusion of charged molecules through the membrane was observed. Above 12.5%, charged dextran of a size of 54.5 nm was able to cross the membrane, implying the formation of pores that exceeded this size (63). Since we observe the permeation toward the small but charged K^+ ion, these thresholds might be different, if they even exist. After 10 min of treatment, we observe 10%–20% of total K release associated with 5%–8% of lipid aldehydes or 0.5%–5% of carboxylic acid formation. It is not clear how the association of a variety of different aldehydes and carboxylic acids might play a role in permeabilization.

Laurdan and di-4-ANEPPDHQ GP were altered differently upon oxidation. This difference might either arise from different locations of the probes in the membrane z axis (38), from the fact that di-4-ANEPPDHQ is leaflet selective and hence might only probe the outer leaflet if there is no flipping (37), or from the fact that both molecules probe different properties (64). The PCA revealed that both probes develop in different directions upon oxidation but also upon the number of lipid unsaturations in the controls. Packing was further no indication of K release except maybe during the formation of hydroperoxides upon post-incubation. The largest changes in GP were observed only for conditions with post-incubation and only in membranes containing polyunsaturated lipids. This implies that certain oxygen addition products strongly alter packing, or the polarity in the vicinity of the fluorophores. Hydroperoxides are supposed to point their hydrophilic peroxyl groups to the membrane interphase, which could alter polarity and packing in the vicinity of the probes (17). The observed changes merit further attention since the use of these probes in more complex membranes might be useful to detect the formation of specific oxidation products.

The release of oxidized lipids from the membrane could have potential impacts in vivo for multiple organisms. During situations of oxidative stress in humans, OxPCs could act as signaling molecules for other distant cells similar to cytokines, such as prostaglandins, which are derived from arachidonic acid. This might especially be true for hydroperoxides that have been shown to induce processes such as ferroptosis (65).

Our observations provide useful insights on how RONS interact directly with cell membranes. This information is especially useful to predict effects on phagocytosed microorganisms, which are subjected to large amounts of RONS produced during the oxidative burst. Since small amounts of oxidized lipids already seem to have an effect on membrane permeability, and especially toward ions that usually maintain the membrane potential, it is foreseeable that ATP production through F-ATPases is compromised because it predominantly relies on the membrane potential component of the proton motive force (66). Lipid oxidation might thus be a very effective way to compromise microorganisms. This principle is used by CAP, which is undergoing many clinical trials on its effectivity on bacterial infections (67–69). CAP is further used in clinical trials, especially for head and neck cancers (70,71). Lipid oxidation could also play an important role here, not only in changing biophysical properties of the membrane but also in producing "signaling" lipid oxides, as discussed before.

All in all, we conclude that there exist probably at least two permeabilization mechanisms in oxidized membranes and that these mechanisms have different dependencies regarding lipid unsaturations, acyl chain asymmetry, and incubation periods.

SUPPORTING MATERIAL

Supporting material can be found online at https://doi.org/10.1016/j.bpj.2023.10.028.

AUTHOR CONTRIBUTIONS

M.X. and E.H.W.K. did the experimental work. M.X., C.A.v.W., A.S., A.F.P.S., E.B., J.A.K., and J.H.L. were involved in the conception of the study. All authors were involved in the design of the manuscript.

ACKNOWLEDGMENTS

We are grateful to Stephan A. Jonker for assisting us in the use of the AAS machine operation, Bonny W. M. Kuipers for support in DLS analysis, and Martin F. Haase as well as Mohd Azeem Khan for providing pendant-drop tensiometry equipment. We further thank the Utrecht University/Einhoven University of Technology Alliance for financing this project. We further are thankful for suggestions and comments provided by Martijn C. Koorengevel. M.X. was supported by a scholarship from the China Scholarship Council (CSC), https://www.chinesescholarshipcouncil.com/, file no. 201809370077.

DECLARATION OF INTERESTS

The authors declare no competing interests.

REFERENCES

1. Chan, H. W. S., D. T. Coxon, …, K. R. Price. 1982. Oxidative reactions of unsaturated lipids. *Food Chem.* 9:21–34.
2. Vona, R., L. Pallotta, …, P. Matarrese. 2021. The impact of oxidative stress in human pathology: Focus on gastrointestinal disorders. *Antioxidants.* 10:201–226.
3. Sultana, S., A. Foti, and J. U. Dahl. 2020. Bacterial defense systems against the neutrophilic oxidant hypochlorous acid. *Infect. Immun.* 88, e00964-19.
4. Brun, P., P. Brun, …, A. Leonardi. 2012. Disinfection of ocular cells and tissues by atmospheric-pressure cold plasma. *PLoS One.* 7, e33245.

5. Babington, P., K. Rajjoub, …, J. H. Sherman. 2015. Use of cold atmospheric plasma in the treatment of cancer. *Biointerphases.* 10, 029403.
6. Laroussi, M., D. A. Mendis, and M. Rosenberg. 2003. Plasma interaction with microbes. *New J. Phys.* 5:41.
7. Ytzhak, S., H. Weitman, and B. Ehrenberg. 2013. The Effect of Lipid Composition on the Permeability of Fluorescent Markers from Photosensitized Membranes. *Photochem. Photobiol.* 89:619–624.
8. van Meer, G., D. R. Voelker, and G. W. Feigenson. 2008. Membrane lipids: where they are and how they behave. *Nat. Rev. Mol. Cell Biol.* 9 (9):112–124.
9. Keweloh, H., and H. J. Heipieper. 1996. Trans unsaturated fatty acids in bacteria. *Lipids.* 31:129–137.
10. Lorent, J. H., and I. Levental. 2019. Preparation and properties of giant plasma membrane vesicles and giant unilamellar vesicles from natural membranes. *In* The Giant Vesicle Book, pp. 21–36.
11. Clemens, M. R., and H. D. Waller. 1987. Lipid peroxidation in erythrocytes. *Chem. Phys. Lipids.* 45:251–268.
12. Ytzhak, S., and B. Ehrenberg. 2014. The effect of photodynamic action on leakage of ions through liposomal membranes that contain oxidatively modified lipids. *Photochem. Photobiol.* 90:796–800.
13. Boonnoy, P., V. Jarerattanachat, …, J. Wong-Ekkabut. 2015. Bilayer Deformation, Pores, and Micellation Induced by Oxidized Lipids. *J. Phys. Chem. Lett.* 6:4884–4888.
14. Bour, A., S. G. Kruglik, …, S. Bonneau. 2019. Lipid Unsaturation Properties Govern the Sensitivity of Membranes to Photoinduced Oxidative Stress. *Biophys. J.* 116:910–920.
15. Bacellar, I. O. L., M. C. Oliveira, …, M. S. Baptista. 2018. Photosensitized Membrane Permeabilization Requires Contact-Dependent Reactions between Photosensitizer and Lipids. *J. Am. Chem. Soc.* 140:9606–9615.
16. Tsubone, T. M., M. S. Baptista, and R. Itri. 2019. Understanding membrane remodelling initiated by photosensitized lipid oxidation. *Biophys. Chem.* 254, 106263.
17. Tsubone, T. M., H. C. Junqueira, …, R. Itri. 2019. Contrasting roles of oxidized lipids in modulating membrane microdomains. *Biochim. Biophys. Acta Biomembr.* 1861:660–669.
18. Reuter, S., T. Von Woedtke, and K. D. Weltmann. 2018. The kINPen - A review on physics and chemistry of the atmospheric pressure plasma jet and its applications. *J. Phys. D Appl. Phys.* 51:233001.
19. Gomes, A., E. Fernandes, and J. L. F. C. Lima. 2005. Fluorescence probes used for detection of reactive oxygen species. *J. Biochem. Biophys. Methods.* 65:45–80.
20. Rouser, G., G. Kritchevsky, …, D. Heller. 1965. Determination of polar lipids: Quantitative column and thin-layer chromatography. *J. Am. Oil Chem. Soc.* 42:215–227.
21. Rouser, G., S. Fkeischer, and A. Yamamoto. 1970. Two dimensional thin layer chromatographic separation of polar lipids and determination of phospholipids by phosphorus analysis of spots. *Lipids.* 5:494–496.
22. Parasassi, T., G. De Stasio, …, E. Gratton. 1990. Phase fluctuation in phospholipid membranes revealed by Laurdan fluorescence. *Biophys. J.* 57:1179–1186.
23. Jin, L., A. C. Millard, …, L. M. Loew. 2006. Characterization and application of a new optical probe for membrane lipid domains. *Biophys. J.* 90:2563–2575.
24. Bligh, E. G., and W. J. Dyer. 1959. Canadian Journal of Biochemistry and Physiology. *Can. J. Biochem. Physiol.* 37:911–917.
25. Haefliger, O. P., and J. W. Sulzer. 2007. Rapid LC-UV-ESI-MS Method to Investigate the Industrial Preparation of Polyunsaturated Fatty Acid Hydroperoxides in Real-Time. *Chromatographia.* 65:435–442.
26. DeLong, J. M., R. K. Prange, …, M. Quilliam. 2002. Using a modified ferrous oxidation-xylenol orange (FOX) assay for detection of lipid hydroperoxides in plant tissue. *J. Agric. Food Chem.* 50:248–254.
27. Andreoli, R., P. Manini, …, W. M. A. Niessen. 2003. Determination of patterns of biologically relevant aldehydes in exhaled breath condensate of healthy subjects by liquid chromatography/atmospheric chemical ionization tandem mass spectrometry. *Rapid Commun. Mass Spectrom.* 17:637–645.
28. Prados, P., T. Fukushima, …, K. Imai. 1997. 4-N,N-Dimethylaminosulfonyl-7-N-(2-aminoethyl)amino-benzofurazan as a new precolumn fluorescence derivatization reagent for carboxylic acids (fatty acids and drugs containing a carboxyl moiety) in liquid chromatography. *Anal. Chim. Acta.* 344:227–232.
29. Ni, Z., B. C. Sousa, …, A. Criscuolo. 2019. Evaluation of air oxidized PAPC: A multi laboratory study by LC-MS/MS. *Free Radic. Biol. Med.* 144:156–166.
30. Ni, Z., G. Angelidou, …, M. Fedorova. 2017. LPPtiger software for lipidome-specific prediction and identification of oxidized phospholipids from LC-MS datasets. *Sci. Rep.* 7 (7):15138–15214.
31. Schmidt-Bleker, A., J. Winter, …, K.-D. Weltmann. 2015. On the plasma chemistry of a cold atmospheric argon plasma jet with shielding gas device. *Plasma Sources Sci. Technol.* 25, 015005.
32. Kowey, P. R. 2002. *In* The Role of Potassium BT - Women's Health and Menopause: New Strategies — Improved Quality of Life, R. A. Lobo, P. G. Crosignani, and …, F. Bruschieds Springer US, pp. 151–157.
33. Volkmar, N., C. M. Gawden-Bone, …, P. J. Lehner. 2022. Regulation of membrane fluidity by RNF145-triggered degradation of the lipid hydrolase ADIPOR2. *EMBO J.* 41, e110777.
34. Ackerman, D., S. Tumanov, …, J. J. Kamphorst. 2018. Triglycerides Promote Lipid Homeostasis during Hypoxic Stress by Balancing Fatty Acid Saturation. *Cell Rep.* 24:2596–2605.e5.
35. Kaiser, H. J., D. Lingwood, …, K. Simons. 2009. Order of lipid phases in model and plasma membranes. *Proc. Natl. Acad. Sci. USA.* 106:16645–16650.
36. Mukherjee, S., and A. Chattopadhyay. 2005. Monitoring the organization and dynamics of bovine hippocampal membranes utilizing Laurdan generalized polarization. *Biochim. Biophys. Acta.* 1714:43–55.
37. Lorent, J. H., K. R. Levental, …, E. Lyman. 2020. Plasma membranes are asymmetric in lipid unsaturation, packing and protein shape. *Nat. Chem. Biol.* 16:710.
38. Suhaj, A., D. Gowland, …, C. D. Lorenz. 2020. Laurdan and Di-4-ANEPPDHQ influence the properties of lipid membranes: A classical molecular dynamics and fluorescence study. *J. Phys. Chem. B.* 124:11419–11430.
39. Bacalum, M., B. Zorilă, and M. Radu. 2013. Fluorescence spectra decomposition by asymmetric functions: Laurdan spectrum revisited. *Anal. Biochem.* 440:123–129.
40. Jurkiewicz, P., L. Cwiklik, …, M. Hof. 2012. Lipid hydration and mobility: An interplay between fluorescence solvent relaxation experiments and molecular dynamics simulations. *Biochimie.* 94:26–32.
41. Navas, J. A., A. Tres, …, F. Guardiola. 2004. Modified ferrous oxidation-xylenol orange method to determine lipid hydroperoxides in fried snacks. *Eur. J. Lipid Sci. Technol.* 106:688–696.
42. Kumari, P., R. P. Singh, …, B. Jha. 2012. Estimation of Lipid Hydroperoxide Levels in Tropical Marine Macroalgae. *J. Phycol.* 48:1362–1373.
43. Spickett, C. M. 2014. The Lipid Peroxidation Product 4-Hydroxy-2-Nonenal: Advances in Chemistry and Analysis. *Redox Biol.* 1:145–152.
44. Sousa, B. C., A. R. Pitt, and C. M. Spickett. 2017. Chemistry and analysis of HNE and other prominent carbonyl-containing lipid oxidation compounds. *Free Radic. Biol. Med.* 111:294–308.
45. Scrimgeour, C. 2005. Bailey's Industrial Oil and Fat Products. *In* Chapter 1: Chemistry of fatty acids.
46. Xia, W., and S. M. Budge. 2017. Techniques for the Analysis of Minor Lipid Oxidation Products Derived from Triacylglycerols: Epoxides, Alcohols, and Ketones. *Compr. Rev. Food Sci. Food Saf.* 16:735–758.
47. Domínguez, R., M. Pateiro, …, J. M. Lorenzo. 2019. A comprehensive review on lipid oxidation in meat and meat products. *Antioxidants.* 8:1–31.
48. Ellis, S. R., H. T. Pham, …, S. J. Blanksby. 2017. Radical Generation from the Gas-Phase Activation of Ionized Lipid Ozonides. *J. Am. Soc. Mass Spectrom.* 28:1345–1358.

49. Zahardis, J., and G. A. Petrucci. 2007. The oleic acid-ozone heterogeneous reaction system: Products, kinetics, secondary chemistry, and atmospheric implications of a model system - A review. *Atmos. Chem. Phys.* 7:1237–1274.

50. Perinelli, D. R., M. Cespi, …, P. Blasi. 2020. Surfactant Self-Assembling and Critical Micelle Concentration: One Approach Fits All? *Langmuir.* 36:5745–5753.

51. Bai, X., L. Xu, …, G. Hu. 2019. Adsorption of Phospholipids at the Air-Water Surface. *Biophys. J.* 117:1224–1233.

52. Pfeiffer, W., T. H. Henkel, …, W. Knoll. 1989. Local Dynamics of Lipid Bilayers Studied by Incoherent Quasi-Elastic Neutron Scattering. *Europhys. Lett.* 8:201–206.

53. Israelachvili, J. 2011. Intermolecular and Surface Forces. Academic Press.

54. Reis, A., and C. M. Spickett. 2012. Chemistry of phospholipid oxidation. *Biochim. Biophys. Acta.* 1818:2374–2387.

55. Squadrito, G. L., R. M. Uppu, …, W. A. Pryor. 1992. Production of the criegee ozonide during the ozonation of 1-Palmitoyl-2-oleoyl-sn-glycero-3-phosphocholine liposomes. *Lipids.* 27:955–958.

56. Bruno, G., S. Wenske, …, K. Wende. 2020. On the Liquid Chemistry of the Reactive Nitrogen Species Peroxynitrite and Nitrogen Dioxide Generated by Physical Plasmas. *Biomolecules.* 10:1687.

57. Nasri, Z., M. Ahmadi, …, K. Wende. 2022. Insight into the Impact of Oxidative Stress on the Barrier Properties of Lipid Bilayer Models. *Int. J. Mol. Sci.* 23:5932.

58. Bacellar, I. O. L., and M. S. Baptista. 2019. Mechanisms of Photosensitized Lipid Oxidation and Membrane Permeabilization. *ACS Omega.* 4:21636–21646.

59. Schnitzer, E., I. Pinchuk, and D. Lichtenberg. 2007. Peroxidation of liposomal lipids. *Eur. Biophys. J.* 36:499–515.

60. Heuvingh, J., and S. Bonneau. 2009. Asymmetric oxidation of giant vesicles triggers curvature-associated shape transition and permeabilization. *Biophys. J.* 97:2904–2912.

61. Wong-Ekkabut, J., Z. Xu, …, L. Monticelli. 2007. Effect of lipid peroxidation on the properties of lipid bilayers: a molecular dynamics study. *Biophys. J.* 93:4225–4236.

62. Paez-Perez, M., A. Vyšniauskas, …, M. K. Kuimova. 2023. Directly imaging emergence of phase separation in peroxidized lipid membranes. *Commun. Chem.* 6:15.

63. Runas, K. A., and N. Malmstadt. 2015. Low levels of lipid oxidation radically increase the passive permeability of lipid bilayers. *Soft Matter.* 11:499–505.

64. Amaro, M., F. Reina, …, E. Sezgin. 2017. Laurdan and Di-4-ANEPPDHQ probe different properties of the membrane. *J. Phys. D Appl. Phys.* 50:134004.

65. Kagan, V. E., G. Mao, …, H. Bayır. 2017. Oxidized Arachidonic/Adrenic Phosphatidylethanolamines Navigate Cells to Ferroptosis. *Nat. Chem. Biol.* 13:81–90.

66. Walker, J. E. 2013. Respiration | F-ATPases. *In* Encyclopedia of Biological Chemistry: Third Edition, 2, pp. 518–523.

67. Isbary, G., G. Morfill, …, W. Stolz. 2010. A first prospective randomized controlled trial to decrease bacterial load using cold atmospheric argon plasma on chronic wounds in patients. *Br. J. Dermatol.* 163:78–82.

68. Klämpfl, T. G., G. Isbary, …, H. U. Schmidt. 2012. Cold atmospheric air plasma sterilization against spores and other microorganisms of clinical interest. *Appl. Environ. Microbiol.* 78:5077–5082.

69. Dijksteel, G. S., M. M. W. Ulrich, …, B. K. H. L. Boekema. 2020. Safety and bactericidal efficacy of cold atmospheric plasma generated by a flexible surface Dielectric Barrier Discharge device against Pseudomonas aeruginosa in vitro and in vivo. *Ann. Clin. Microbiol. Antimicrob.* 19:1–10.

70. Semmler, M. L., S. Bekeschus, …, L. Boeckmann. 2020. Molecular Mechanisms of the Efficacy of Cold Atmospheric Pressure Plasma (CAP) in Cancer Treatment. *Cancers.* 12.

71. Von Woedtke, T., H. R. Metelmann, and K. D. Weltmann. 2014. Clinical Plasma Medicine: State and Perspectives of in Vivo Application of Cold Atmospheric Plasma. *Contrib. Plasma Phys.* 54:104–117.